Grid-Supportive Loads - A New Approach to Increasing Renewable Energy in Power Systems

Himanshu Jain[1,2], *Member, IEEE*, Barry Mather[2], *Senior Member, IEEE*, Akshay Kumar Jain[2,3], *Student Member, IEEE*, and Samuel F. Baldwin[4], *Life Member, IEEE*

***Abstract*—This paper demonstrates the potential of inverter-based loads to support grid reliability during power system transients thereby enabling reliable integration of renewable energy in power systems. Such loads are referred to in this paper as grid-supportive loads (GSLs). A new GSL model is developed that simulates the transient response capabilities that can be programmed in electronic loads. The model's design enables it to be easily integrated in widely used commercial power system transient analysis software. Theoretical expressions are derived that explain the workings of the GSL model. The performance, numerical stability, and impact of the GSL model is validated on 9-bus and 2000-bus synthetic power system models using generator tripping and bus fault disturbances. Results on the 2000 bus system show that in the absence of frequency support from wind/solar generation resources, just 20% of loads with grid-supportive capabilities can improve frequency response by up to 2000 MW/0.1 Hz and reduce deviation in frequency at nadir by up to 60% compared to the situation when GSLs are absent. Power system reliability also improves under fault events. It is further shown that GSLs can aid in integrating more renewable generation without degrading the overall transient response of the power system.**

***Index Terms*— electric vehicles, inverters, load modeling, power system dynamics, power system modeling, power system stability, renewable energy resources, solar power generation, wind power generation**

I. Introduction

Increasing integration of inverter-based generation resources (IBRs) in power systems has necessitated the development of grid-supportive controls in these resources. Voltage ride-through, volt-var control, and power-frequency droop response are some of the capabilities that have already been incorporated or are expected to be incorporated soon in IBRs [1]–[3]. Simulation models incorporating these controls in IBRs have also been developed for both transmission and distribution systems for steady-state and dynamic analyses [4]–[6].

Profound changes are also taking place in the end-use loads. The increased prevalence of power electronic grid interfaces of some of the largest loads such as electric motors, air conditioners and refrigerators, and integration of electric vehicles is already taking place and is expected to gather pace in the foreseeable future [7]. These power electronic loads (also referred to as inverter-based loads in this paper) offer an opportunity to provide grid support [8]. It is likely easy to add control functionality to make them responsive to grid-relevant values, like voltage and frequency in the transient timescale with little to no impact to the end-user's utility of the electrical load. Such electronic loads are referred to in this paper as grid-supportive loads or GSLs.

The research presented in this paper is novel because little research has been done on exploring the potential of electronic loads for providing grid-support in power system transient timeframe (milliseconds to few seconds). There are programs such as the Electricity Reliability Council of Texas or ERCOT Load Resource program, where loads trip automatically if the frequency falls below a certain level, but these loads only respond in emergency situations and cannot help during over-frequency conditions. Moreover, inverter-based loads such as variable frequency drives can trip once terminal voltage falls below a threshold, but this support is neither under a user's control nor available when the voltage or frequency changes are within the tripping thresholds.

Research has also been done on controlling loads, such as thermostatically controlled loads, to provide demand response in the minutes to hours timeframe based on control signals (pre-programmed or real-time) received from the electric utility or a third party aggregator [9], [10], or by reducing voltages as part of conservation voltage reduction programs [11]–[13]. However, in the transient timeframe an autonomous response driven by only local measurements is required for straightforward, low-cost implementation and to avoid the cybersecurity concerns that come from communications-based control methods.

Literature review further showed that existing load

This work was authored by the National Renewable Energy Laboratory, operated by Alliance for Sustainable Energy, LLC, for the U.S. Department of Energy (DOE) under Contract No. DE-AC36-08GO28308. The U.S. Government retains and the publisher, by accepting the article for publication, acknowledges that the U.S. Government retains a nonexclusive, paid-up, irrevocable, worldwide license to publish or reproduce the published form of this work, or allow others to do so, for U.S. Government purposes. The views expressed in the article do not necessarily represent the views of the DOE or the U.S. Government.

[1]Himanshu Jain is with the Indian Institute of Technology, Roorkee, Uttarakhand, India. He was with the National Renewable Energy Laboratory (NREL), Golden, CO, USA, 80401 when this research was completed (e-mail: himanshu.jain@hre.iitr.ac.in).

[2]Barry Mather is with the National Renewable Energy Laboratory (NREL), Golden, CO, USA, 80401 (e-mail: barry.mather@nrel.gov)

[3]Akshay Jain is at Virginia Tech, Blacksburg, VA, USA, 24060. He was with the National Renewable Energy Laboratory (NREL), Golden, CO, USA, 80401 when this research was completed (e-mail: akjain@vt.edu).

[4]Samuel F. Baldwin is with the Office of Energy Efficiency and Renewable Energy Office at the U.S. Department of Energy, Washington, DC, USA 20585 (e-mail: sam.baldwin@ee.doe.gov).

modeling research can be classified into three key categories. The first category includes research aimed at obtaining good models of power and energy consumed by loads without consideration of the loads' electrical behavior [14]–[17]. In the second category are those research efforts, where obtaining steady state electrical models of loads (valid for minutes to hours timescale) was the objective [18]–[21]. Finally, the third category includes load modelling research aimed at obtaining transient models of loads [22]–[26]. This category also includes the development of the Western Electricity Coordinating Council (WECC) composite load model (CLM), WECC-CLM, which is one of the most detailed load models currently used for research and in industry [26]. Although voltage dependent response of electronic loads is included in the WECC-CLM, current limits of electronic loads and their potential to provide automatic frequency response are not modeled. A major gap in these research efforts is the focus on obtaining the behavior of *existing* loads, and not on developing models that can demonstrate the potential of inverter-based loads to provide grid support in the transient timeframe.

To summarize, literature review has revealed the following research gaps: (i) capabilities of inverter-based loads to provide autonomous response at transient timeframe and also support variable renewable energy integration have not been explored, and (ii) models that can be used to investigate the realizable grid-supportive capabilities of inverter-based loads at transient timeframes are not available.

The research presented in this paper addresses these gaps by (i) developing a GSL model that can respond autonomously in the transient timeframe based on local measurements and (ii), by demonstrating using a 2000 bus dynamic model with over 1100 instances of the developed GSL model that GSLs can help in integrating more renewable energy in power systems without requiring grid support from renewable generation resources.

This paper is divided into seven sections. Section II explains the electronic load model of the WECC-CLM and highlights its limitations. Section III presents the novel GSL model and explains its features. In section IV, theoretical analysis explaining the workings of the GSL model under generator tripping events is presented. Section V presents the validation results for the developed GSL model. In section VI, the ability of GSLs in increasing variable renewable energy integration is demonstrated on a synthetic, 2000 bus model of the Electric Reliability Council of Texas (ERCOT) for generator tripping and fault events. Section VII concludes the paper and provides future research directions.

II. Limitations of Electronics Load Modelling in WECC-CLM

WECC-CLM is a comprehensive dynamic load model that is used in industry and for research to simulate the aggregate dynamic response of distribution system connected loads and distributed generators [26]. Recently, a detailed model for distributed generators called DER_A was included in the WECC-CLM [27]. The main components of the composite load model are:

1. Distribution substation transformer
2. Equivalent feeder model
3. Motor model (Four types of motors – A to D)
4. Static load model
5. Distributed generator model
6. Electronic load model

In recent years, the main drivers for using WECC-CLM have been (i) fault-induced delayed voltage recovery (FIDVR) studies [28], [29], and (ii) improving the accuracy of distributed generation dynamics modeling [30]. The component of the WECC-CLM that has received little attention is the electronic load model. As described in [31], the electronic load model in the WECC-CLM is used to model all power electronic or inverter-interfaced loads. The electronic load behaves as a fixed power factor (typically unity), constant power load until the voltage drops to breakpoint 1, V_{d1}, beyond which the fraction of online electronic load is linearly curtailed until it becomes zero at the second voltage breakpoint, V_{d2}. The amount of electronic load that should recover as the voltage exceeds V_{d2} can also be specified. The restoration is linear between V_{d2} and V_{d1}, and beyond V_{d1} the allowed fraction of load recovers.

The simplicity of electronic load modelling in the WECC-CLM does not allow the investigation of the full range of grid-supportive behavior that can be obtained from electronic loads. The main limitations of the electronic load model in the WECC-CLM are:

1. Inability to model frequency response from loads.
2. No option to add delays after which loads should trip on account of low voltages. Loads start tripping immediately as the V_{d1} threshold is reached. As shown in [32], inverter-based loads such as variable frequency drives can ride-through deep voltage sags (up to zero voltage) of varying durations.
3. Inability to recover load after it is shed based on grid conditions or after a fixed delay to simulate a compromise between serving the desired load and supporting the grid.
4. There is no provision to provide overcurrent limits for electronic loads. If V_{d1} is low enough, constant power load behavior will result in large current being drawn by the electronic load, which may not be realistic because power electronics devices typically have limited overcurrent capabilities.

That the WECC-CLM is a state-of-the-art load model used for research today and the GSL behavior is not modeled in it is further supported by recent publications as discussed next.

In [33], a new load model was presented that combined constant impedance (Z), constant current (I), constant power (P) or ZIP load with an electronic load model, which was similar to the electronic load model found in the WECC-CLM. The proposed load model was called the composite electronic ZIP load model or CEZLM. While the objective of the paper was to use phasor measurement units to obtain the parameters of CEZLM in real time, no consideration was given to the grid supportive capabilities of electronic loads. Moreover, no frequency-based load modulation, droop-based or otherwise, was considered. In [34], "*An updated model with variable frequency drive is formulated to reproduce the load behavior of modern electricity consumers*". Scalar Volt/Hz control strategy was modeled for the variable frequency drive (VFD) and no

consideration for explicit grid supportive behavior was provided in the proposed model. Frequency dependence of ZIP loads was also not considered. The status of the WECC-CLM as the state-of-the-art load model was further affirmed in [35], where a method to reducing the parameters of the WECC-CLM (named cmpldwg in GE-PSLF®) was proposed. No grid supportive capabilities from the electronic loads were proposed in this paper. In [36], a simple composite load model comprising of ZIP model and induction machine model was proposed followed by development of techniques to identify its parameters. It was stated in the conclusion that the approach presented in the paper would be extended to identify the parameters of the WECC-CLM. This further affirms that the WECC-CLM is the state-of-the-art load model and load models being proposed thus far have not explored the potential of electronic loads to provide grid support. In [37] an algorithm to estimating the parameters of the WECC-CLM was proposed. The WECC-CLM was referred to as an advanced load model in this paper. In [38], a two-stage WECC-CLM composition and parameter estimation approach was presented, and no grid supportive feature was proposed to be included in the model. In [39], a performance-based model for representing the aggregate behavior of VFDs was proposed because the existing electronic load model in the CLM was found to be inadequate in capturing transients associated with VFDs. However, the proposed model did not include frequency-based grid support or provisions to limiting the duration of grid support. The performance of the proposed model to changes in frequency was also not tested and left for future.

A novel GSL model is presented next that addresses the four limitations of the WECC-CLM listed earlier.

III. A New Grid-Supportive Load Model

A. GSL Model

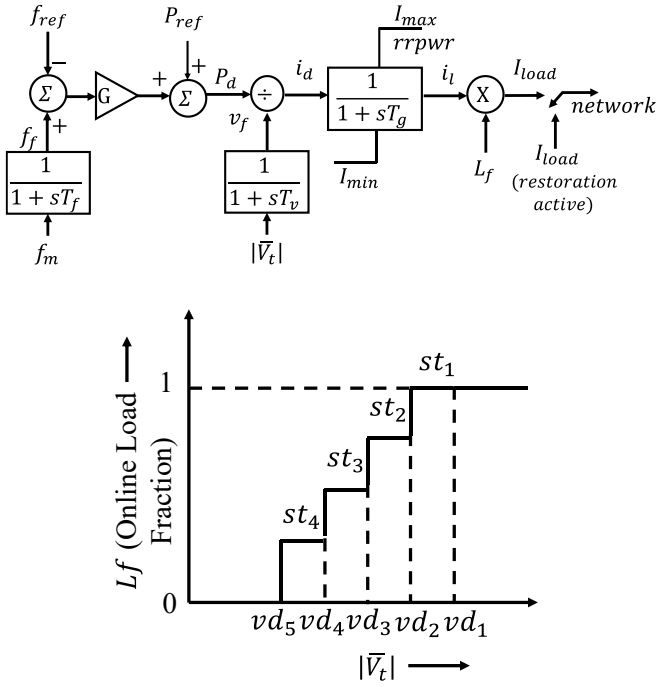

Figure 1. Grid-supportive load model

The block diagram of the GSL model is shown in Figure 1. This model assumes that the power factor of the electronic load is unity, although changing the model to allow a non-unity power factor is straightforward. The GSL model is explained mathematically here with the qualitative description provided in Appendix I.

The GSL model has five modules that work together to address the four limitations of the WECC-CLM. The "s" in Figure 1 indicates that the block should be interpreted as the Laplace transform of a differential equation. The five modules are:

Voltage and frequency measurements:

$$\frac{d_{f_f}}{dt} = \left(\frac{1}{T_f}\right)(f_m - f_f) \tag{1}$$

$$\frac{d_{v_f}}{dt} = \left(\frac{1}{T_v}\right)(|\bar{V}_t| - v_f) \tag{2}$$

Frequency-power relationship:

$$P_d = \left(\frac{100}{R}\right)(f_f - f_{ref}) + P_{ref} \tag{3}$$

Inverter Model:

$$i_d = \frac{P_d}{v_f} \tag{4}$$

If $v_f = 0, then\ v_f = 0.001\ p.u.$ to prevent division by zero.

$$\left.\begin{aligned} &\frac{d_{i_l}}{dt} = \left(\frac{1}{T_g}\right)(i_d - i_l) \\ &\text{If } i_l > 0 \text{ and } \frac{d_{i_l}}{dt} \geq rrpwr, then: \\ &\frac{d_{i_l}}{dt} = rrpwr \\ &\text{Else if } i_l < 0 \text{ and } \frac{d_{i_l}}{dt} \leq -rrpwr, then: \\ &\frac{d_{i_l}}{dt} = -rrpwr \\ &\text{Else if } i_l > I_{max} \text{ and } \frac{d_{i_l}}{dt} > 0, then: \\ &\frac{d_{i_l}}{dt} = 0 \\ &i_l = I_{max} \\ &\text{Else if } i_l < I_{min} \text{ and } \frac{d_{i_l}}{dt} < 0, then: \\ &\frac{d_{i_l}}{dt} = 0 \\ &i_l = I_{min} \end{aligned}\right\} \tag{5}$$

$$I_{load} = i_l * L_f \tag{6}$$

Load restoration:

$$\left.\begin{aligned} If\ t_{sim} > Tlrest\ and \frac{\left|P_{load_{GSL}} - P_{ref}\right|}{P_{ref}} > 0.05, then \\ I_{load} = \frac{P_{load_{GSL}} + rrate * \Delta T}{|\bar{V}_t|} \end{aligned}\right\} \tag{7}$$

Voltage dependent load tripping logic:

N stages are defined such that the i^{th} stage (st_i) is activated if:

$$st_i\ active: vd_{i+1} < |\bar{V}_t| \leq vd_i \tag{8}$$

Once the i^{th} stage is active, then:

This article has been accepted for publication in a future issue of this journal, but has not been fully edited. Content may change prior to final publication. Citation information: DOI 10.1109/TSG.2022.3153230, IEEE Transactions on Smart Grid

$$\left.\begin{array}{c} if\ tpu_i > Tpu_i\ then\ L_f = Lf_i \\ if\ |\bar{V}_t| \geq vd_i, then: \\ trst_i = trst_i + \Delta T \\ tpu_i = tpu_i + \Delta T \\ if trst_i > Trst_i, then: \\ tpu_i = 0 \\ trst_i = 0 \\ L_f = Unchanged \end{array}\right\} \quad (9)$$

Table I. Symbols used in GSL Model Description

Symbol	Definition	Symbol	Definition	Symbol	Definition
f_f	Measured frequency (p.u.)	I_{min}	Minimum current limit of the GSL (p.u.)	vd_{i+1}	Lower voltage limit of i^{th} stage of voltage-dependent trip logic (p.u,)
v_f	Measured voltage magnitude (p.u.)	I_{max}	Maximum current limit of the GSL (p.u.)	vd_i	upper voltage limit of i^{th} stage of voltage-dependent trip logic (p.u.)
f_m	Load bus frequency (p.u.)	T_g	Inverter time constant (sec)	tpu_i	i^{th} stage pick-up timer (sec)
$\|\bar{V}_t\|$	Load bus voltage magnitude (p.u.)	$rrpwr$	Maximum ramp rate	Tpu_i	i^{th} stage pick-up time (60/50 Hz cycles)
T_f	Frequency transducer time constant (sec)	t_{sim}	Simulation time	$trst_i$	i^{th} stage reset timer
T_v	Voltage transducer time constant (sec)	ΔT	Simulation time step	$Trst_i$	i^{th} stage reset time (60/50 Hz cycles)
R	GSL droop coefficient; $G = 100/R$	$Tlrest$	Time after which GSL load may start to be restored	L_f	Load fraction that stays online
f_{ref}	Initial load bus frequency (p.u.)	$P_{load_{GSL}}$	Current power demand of the GSL (p.u.)		
P_{ref}	Initial power demand of GSL (p.u.)	$rrate$	Ramp rate at which GSL is restored (p.u./sec)		

B. Initialization of the GSL Model

Under the assumption that the GSL model is operating in the linear region and the pre-disturbance voltages are above the highest voltage-dependent trip logic voltage level, initialization of the GSL model can be performed by setting the derivatives of (1), (2) and (5) to zero. This results in (10).

$$\left.\begin{array}{c} f_f = f_m \\ v_f = |\bar{V}_t| \\ i_d = i_l \end{array}\right\} \quad (10)$$

Because i_l is obtained from the network power flow solution at the time of initialization as $i_l = \frac{P_{ref}}{|\bar{V}_t|}$ (power factor of GSLs is assumed to be unity), using (10), (11) is obtained:

$$i_l = i_d = \frac{P_{ref}}{v_f} \quad (11)$$

Using (11) and (4), $P_{ref} = P_d$. Substituting $P_{ref} = P_d$ in (3) and using (10) gives (12).

$$f_{ref} = f_m \quad (12)$$

Therefore, the initial states of three state variables are as given in (13):

$$\begin{bmatrix} f_f \\ v_f \\ i_l \end{bmatrix} = \begin{bmatrix} f_m \\ |\bar{V}_t| \\ \frac{P_{ref}}{|\bar{V}_t|} \end{bmatrix} \quad (13)$$

Because dynamic simulations are typically initialized assuming 60 or 50 Hz grid frequency at all buses, $f_m = 1\ p.u.$ at initialization.

IV. Theoretical Analysis of the GSL Dynamic Model

In this section, analytical expressions are derived to estimate the system-wide frequency response in the presence of GSLs for generator tripping events. This model provides insights into the workings of the developed GSL model and explains the reasons for the improvement in frequency response of the 2000 bus synthetic, ERCOT-inspired model discussed in Section VI. Moreover, the approach and the expressions developed in this section enable estimation of frequency nadirs and settling frequencies under generator tripping events without running detailed dynamic simulations.

A. Primary Assumptions for the Power System Model

Let us assume that the power system has a copper plate network. This is a valid assumption for a generator tripping event where the amount of generation lost is a small fraction of the total system generation because the network real and reactive power losses will be small when compared to the total power delivered. For the same reasons, the effect of rotor electrical circuit can be ignored, and constant field excitation voltage can be assumed. As a result, network voltages can be assumed to be unchanged before and after the generator tripping event. Because of the unchanged voltages, real and reactive powers consumed by the loads, and renewable generators power output before and after the generator tripping event can also be assumed to remain unchanged (frequency response is not provided by the renewable plants).

B. Two Governor-Generator Model

Above assumptions enable the modeling of power system dynamics using two governor-generator models connected in parallel, with the entire network reduced to real and reactive power demand at the terminals of the two generators. Because the generators have high power factors and voltage magnitudes are not assumed to change, only the real power demand is modeled at the generators' terminals. Very small stator resistance compared to stator reactance means that real power

demand can be assumed to change only because of the GSLs. The resulting equivalent model of the power system is shown in Figure 2. Because GGOV1 is a generic turbine-governor model, the derivation that follows uses the GGOV1 dynamics with droop control enabled ($rselect$ flag is set to 1) [40]. It is further assumed that only the part of the GGOV1 model shown in Figure 2 contributes to its dynamic response. The two generators terminate at the same terminals, where aggregate renewable generation and aggregate GSL and non-GSL loads are also connected. Secondary frequency response is assumed to be absent.

C. Derivation of Deviation in Angular Frequency

Table II. Definitions of Symbols used in the Derivation

Symbol	Definition
G_t	Generator that trips
G_o	Generator that stays online after the disturbance
S_B	Aggregate MVA base of all the synchronous generators
S_{GSL}	Aggregate MVA base of GSLs (MVA)
ω_s	Steady state angular frequency (p.u.)
P_0	Pre-disturbance, aggregate steady state power supplied by G_o and G_t (MW)
$P_{0_{p.u.}}$	Pre-disturbance, aggregate steady state power supplied by G_o and G_t (p.u.)
P_{tr}	Power generated by G_t at the pre-disturbance steady state (MW)
P_{G_o}	Power generated by G_o at the pre-disturbance steady state (MW)
P_{elec_o}	Power generated by G_o at the pre-disturbance steady state (p.u.); $P_{elec_o} = P_{G_o}/S_B$
P_{ref_o}	G_o governor's reference power (p.u.)
P_{m_o}	Pre-disturbance mechanical power output from G_o's turbine/governor (p.u.)
ΔP_{m_o}	Change in mechanical power output of the governor of G_o (p.u.)
$P_{tr_{p.u.}}$	Pre-disturbance steady state power generated by G_t (p.u.)
P_{ref}	Aggregate initial power demand of GSLs (p.u.)
P_{GSL}	Aggregate power demand of GSLs (MW)
$P_{non-GSL}$	Aggregate power demand of non-GSLs (MW)
P_{ren}	Aggregate power generation of renewable generators (MW)
P	Electrical power demand on G_0 at time t after G_t trips (MW)
$P_{p.u.}$	Electrical power demand on G_0 at time t after G_t trips (p.u.)
ω	Angular frequency of G_o at time t
$\Delta\omega$	Rotor speed deviation of G_0; $\Delta\omega = \omega - \omega_s$
ΔP_{GSL}	Aggregate change in power demand of the GSLs after the disturbance (p.u.)
R_{GSL}	Aggregated droop coefficient of the GSLs
H_{eq}	Inertia constant of G_o
r	G_o governor's droop constant (p.u.)
$Tpelec$	G_o governor's power transducer time constant (sec)
K_{pgov}	G_o governor's PI controller proportional gain
K_{igov}	G_o governor's PI controller integral gain
T_{act}	G_o governor's actuator time constant (sec)
K_{turb}	G_o governor's turbine gain
T_b	G_o governor's turbine lag time constant (sec)

Given the definitions of G_o, P_0, P_{elec} and P_{tr}, P_{G_o} can be written as (14).

$$P_{G_o} = P_0 - P_{tr} \tag{14}$$

Again, based on the definitions in Table II, P_{GSL} can be written as (15).

$$P_{GSL} = P_{ref} * S_{GSL} \tag{15}$$

At the pre-disturbance steady state, using (15) and real power balance we can write (16).

$$P_0 = P_{GSL} + P_{non-GSL} - P_{ren}$$
$$\Longrightarrow P_{non-GSL} - P_{ren} = P_0 - P_{ref} * S_{GSL} \tag{16}$$

Because of the assumptions listed earlier, namely (i) network voltages can be assumed to be unchanged before and after the generator tripping event, and (ii) frequency response is not provided by the renewable generators, (16) holds after G_t trips.

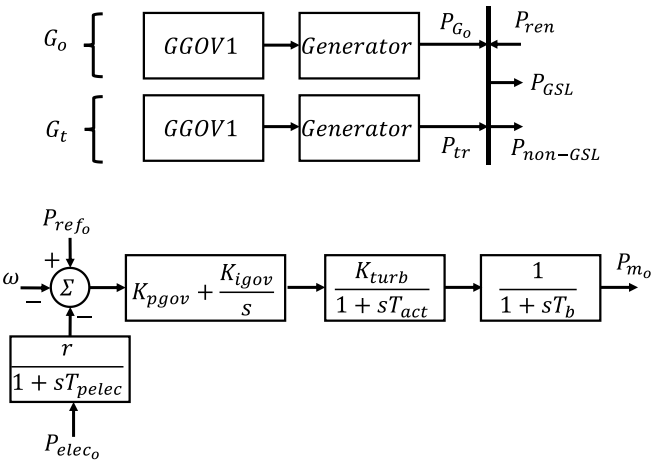

Figure 2. Two Governor-Generator Model (Top). Droop portion of the GGOV1 turbine-governor model (Bottom).

From the GGOV1 dynamic model shown in Figure 2 corresponding to the turbine/governor of G_o, the input to the PI controller block must be zero at the pre-disturbance steady state. Therefore, (17) must hold.

$$P_{ref_o} = rP_{elec_o} + \omega_s \tag{17}$$

P_{ref_o} remains unchanged during the dynamic simulation because secondary frequency response is assumed to be absent.

Using (14) and the definition of P_{elec_o} from Table II, (17) can be written as (18).

$$P_{ref_o} = \frac{r(P_0 - P_{tr})}{S_B} + \omega_s \tag{18}$$

Once the generator generating P_{tr} trips, both the generator and its governor go offline instantaneously or a step-change of P_{tr} occurs and the output mechanical power of the system becomes P_{G_o}. At the same time, using (16) and real power balance of the system wide electrical power demand, P can be written as (19).

$$P = P_{GSL} + P_{non-GSL} - P_{ren}$$
$$= \left(P_{ref} + \Delta P_{GSL}\right)S_{GSL} + P_0 - P_{ref} * S_{GSL}$$
$$= P_0 + \Delta P_{GSL}S_{GSL} \tag{19}$$

If the voltage and frequency sensor time constants are ignored in the GSL model of Figure 1, ΔP_{GSL} can be written as (20) using Laplace transform.

$$\Delta P_{GSL}(s) = \frac{R_{GSL}}{1 + sT_G}\Delta\omega(s) \tag{20}$$

Converting P to p.u. by dividing (19) by S_B, taking the Laplace Transform of the resulting expression, and using (20), (21) is obtained.

$$\frac{P(s)}{S_B} = \frac{P_0(s)}{S_B} + \frac{R_{GSL}}{1+sT_G}.\frac{S_{GSL}}{S_B}.\Delta\omega(s)$$
$$\Rightarrow P_{p.u.}(s) = P_{0_{p.u.}}(s) + \frac{R_{GSL_{eq}}}{1+sT_G}\Delta\omega(s) \quad (21)$$

where, $R_{GSL_{eq}} = R_{GSL}\left(\frac{S_{GSL}}{S_B}\right)$ is the equivalent droop coefficient of all the GSLs.

From (21) and Figure 2, the input signal $u(s)$ to the PI controller block of governor of G_o is given by (22).

$$u(s) = \left(P_{ref_o}(s) - \omega(s) - \left(\frac{r}{1+sT_{pelec}}\right)\left(P_{0_{p.u.}}(s) + \frac{R_{GSL_{eq}}}{1+sT_G}\Delta\omega(s)\right)\right) \quad (22)$$

(22) can also be written as (23).

$$u(s) = \left(P_{ref_o}(s) - \frac{r}{1+sT_{pelec}}\left(P_{0_{p.u.}}(s) - P_{tr_{p.u.}}(s)\right) - \omega_s(s)\right) + \omega_s(s) - \omega(s) - \frac{r}{1+sT_{pelec}}\left(P_{tr_{p.u.}}(s) + \frac{R_{GSL_{eq}}}{1+sT_G}\Delta\omega(s)\right)$$
$$= u_0(s) + \Delta u\,(s) \quad (23)$$

where,

$$u_0(s) = \left(P_{ref_o}(s) - \frac{r}{1+sT_{pelec}}\left(P_{0_{p.u.}}(s) - P_{tr_{p.u.}}(s)\right) - \omega_s(s)\right)$$

and

$$\Delta u(s) = \omega_s(s) - \omega(s) - \frac{r}{1+sT_{pelec}}\left(P_{tr_{p.u.}}(s) + \frac{R_{GSL_{eq}}}{1+sT_G}\Delta\omega(s)\right).$$

Carefully examining $u_0(s)$ reveals that it is the pre-disturbance input to the PI controller block of the governor of G_o, and hence it must be zero. $\Delta u(s)$ is the change in the input to the PI controller that will change the electrical power output of G_o and can be written as (24).

$$\Delta u(s) = -\Delta\omega(s) - \frac{r}{1+sT_{pelec}}\left(P_{tr_{p.u.}}(s) + \frac{R_{GSL_{eq}}}{1+sT_G}\Delta\omega(s)\right) \quad (24)$$

Because $P_{tr_{p.u.}}(s)$ is a step function, its Laplace Transform should be written as $\frac{P_{tr_{p.u.}}}{s}$. Therefore, (24) becomes (25).

$$\Delta u = -\Delta\omega(s)\left(1 + \frac{r}{1+sT_{pelec}}.\frac{R_{GSL_{eq}}}{1+sT_G}\right) - \frac{r}{1+sT_{pelec}}.\frac{P_{tr_{p.u.}}}{s} \quad (25)$$

If $x = \left(1 + \frac{r}{1+sT_{pelec}}.\frac{R_{GSL_{eq}}}{1+sT_G}\right)$ and $y = \frac{r}{1+sT_{pelec}}.\frac{P_{tr_{p.u.}}}{s}$, then using (25) and the GGOV1 model of Figure 2, ΔP_{m_o} can be written as (26).

$$\Delta P_{m_o} = -K_{turb}.x.z.\Delta\omega - y.K_{turb}.z \quad (26)$$

where, $z = \left(K_{pgov} + \frac{K_{igov}}{s}\right)\left(\frac{1}{1+sT_{act}}\right)\left(\frac{1}{1+sT_b}\right)$

Because the pre-disturbance mechanical power input to the online synchronous generator is $P_0(p.u.) - P_{tr}(p.u.)$ and the change in mechanical power input after the disturbance is ΔP_{m_o}, using (21) and the definition of $\Delta\omega$, the rotor speed differential equation for the online synchronous generator can be written in Laplace domain as (27), which after rearrangement of the terms results in $\Delta\omega(s)$ being given by (28).

$$\mathcal{L}\left(\frac{2H_{eq}}{\omega_s}\left(\frac{d\omega}{dt}\right)\right) = \left(P_{0_{p.u.}}(s) - P_{tr_{p.u.}}(s) + \Delta P_{m_o}(s)\right) - P_{0_{p.u.}}(s) - \frac{R_{GSL_{eq}}}{1+sT_G}\Delta\omega(s)$$
$$\Rightarrow s\frac{2H_{eq}\Delta\omega(s)}{\omega_s} = \Delta P_{m_o}(s) - \frac{P_{tr}}{s} - \frac{R_{GSL_{eq}}}{1+sT_G}\Delta\omega(s) \quad (27)$$
$$\Longrightarrow \Delta\omega(s) = -\frac{P_{tr_{pu}}.expr1}{expr2} \quad (28)$$

where, the expressions for $expr1$ and $expr2$ are given in Appendix II.

Simplifying $\frac{expr1}{expr2}$, $\Delta\omega(s)$ can be written as (29). Expressions for coefficients $a_0 - a_5$ and $b_0 - b_6$ are also provided in appendix II.

$$\Delta\omega(s) = -\frac{P_{tr_{p.u.}}(a_5s^5 + a_4s^4 + a_3s^3 + a_2s^2 + a_1s + a_0)}{2H_{eq}s(b_6s^6 + b_5s^5 + b_4s^4 + b_3s^3 + b_2s^2 + b_1s + b_0)} \quad (29)$$

While the exact nature of the roots/poles of (29) cannot be known without substituting the numerical values of the parameters, the complex conjugate roots theorem assures that because all the coefficients of the denominator of (29) are real, its complex roots will always appear as complex conjugate pairs.

However, an analytical expression, (30), for the final post-disturbance steady state can be obtained from (29) under the assumption that $\Delta\omega(s)$ has at most one zero on the origin and all non-zero roots have negative real parts.

$$\Delta\omega_{final} = \lim_{s\to 0} s\Delta\omega(s) = \frac{-P_{tr_{p.u.}}}{2H_{eq}}\frac{a_0}{b_0}$$
$$= -P_{tr_{p.u.}}\frac{K_iK_tr}{K_iK_t + K_iK_trR_{GSL_{eq}}}$$
$$\Longrightarrow \Delta\omega_{final} = -P_{tr_{p.u.}}\left(\frac{1}{\frac{1}{r} + R_{GSL_{eq}}}\right) \quad (30)$$

The expression for $\Delta\omega_{final}$ in (30) shows that the impact of the GSLs is to reduce the overall frequency-power droop in the power system, which results in faster response, higher nadir, and higher settling frequencies.

This derivation is validated using the data from the ERCOT2K System in section VI.

V. GSL Model Validation

The results presented in this section serve two purposes. First, they validate the model behavior by showing that it performs as designed. Secondly, they show the relative improvement in grid performance because of the addition of the

developed GSL model.

Simulations are performed using the WECC 9-bus system model [41]. 80% of the load at bus 5 is modeled as non-electronic load using the WECC-CLM model. Remaining 20% load is either modeled using the electronic load model of the WECC-CLM or using the proposed GSL model of Figure 1. Two disturbances are simulated – tripping of 71.6 MW generator at bus 1 and three-phase bolted fault at bus 6 that lasts for 0.1 seconds. The base parameter names and values of the GSL model are listed in Table III.

Table III. GSL model base parameters

Name	Value	Name	Value	Name	Value
$Rated\ MVA$	20 MVA	I_{min}	0.0 p.u.	$Tpu3$	2 cycles
T_f	0.05 s	vd_1	0.7 p.u.	$Trst$	2 cycles
T_v	0.05 s	vd_2	0.4 p.u.	Lf_1	0.8
R	5.0	vd_3	0.2 p.u.	Lf_2	0.4
T_g	0.02 s	vd_4	0.0 p.u.	Lf_3	0.0
$rrpwr$	1 (100%/s)	$Tpu1$	10 cycles	$Tlrest$	100 s
$Imax$	1.1 p.u.	$Tpu2$	4 cycles	$rrate$	10 (10%/s)

The following 50 seconds long simulations are performed (1-4 for generator tripping event and 5-10 for fault event):

1. Without GSL
2. With GSL, base parameters of Table III
3. With GSL, load restoration enabled ($Tlrest = 10\ s$)
4. With GSL, load restoration enabled ($Tlrest = 10\ s$, $rrate = 1$%/s)
5. Without GSL
6. With GSL, base parameters of Table III
7. With GSL, high I_{max} (3.0 p.u.)
8. With GSL, medium I_{max} (1.5 p.u.)
9. With GSL, lower stage 1 pickup time ($Tpu1 = 4$ cycles)
10. With GSL, load restoration enabled ($Tlrest = 10\ s$)

Voltages and frequencies at bus 5 and powers absorbed by the GSL at bus 5 for all generator tripping and fault simulations are plotted separately in Figure 3 and Figure 4, respectively. The key observations from the figures are discussed next.

A. Observations Validating the GSL Model (Generator Tripping Event)

In simulation 2, the reduction in load is according to the selected value of R (5%). This is because the frequency nadir is 57.93 Hz and the load nadir is 7.73 MW, which implies that for the drop of 2.07 Hz or 3.45%, the decrease in load was 69%.

The frequency and GSL power nadirs for simulation 3 are identical to those observed in simulation 2 because the two simulations are identical except that load restoration is enabled in simulation 3.

Moreover, in simulation 3, load is restored to its pre-disturbance value around 10 seconds after the load first changes by more than 5% from its initial value, which is the expected response as per the GSL model design.

The load restoration feature is further validated in simulation 4, where load recovery is around 10 times slower compared to simulation 3. After 11.3 seconds when load restoration starts, it takes 2.8 seconds for it to recover in simulation 3 compared to 27.9 seconds in simulation 4.

B. Observations Validating the GSL Model (Fault Event)

The feature of the GSL that simulates the maximum current limits of electronic loads is validated in simulations 6-10. Simulations 7 and 8 show that by increasing the maximum overcurrent limit to 3.0 and 1.5 times the rated value, respectively electronic load "clipping" is avoided unlike simulations 6, 9 and 10, where load is clipped.

The voltage-based tripping behavior is validated by simulation 9, where voltage remains below 0.7 p.u. for more than 3 cycles resulting in 20% of the load to trip or 80% of the load staying online. As a result, highest frequency nadir and settling frequency are obtained for this simulation when compared with simulations 6, 7, 8 and 10.

C. Observations Showing Differences in Grid Impact between the GSL Model and the WECC-CLM

In simulation 1, the frequency nadir is >0.6 Hz lower compared to the frequency nadir in simulations 2-4, where load was modeled using the proposed GSL model. This indicates that loads with the proposed GSL behavior can provide more grid support compared to electronic loads with same characteristics as the electronic load model of the WECC-CLM. This observation also shows that the proposed GSL model can enable the simulation of significantly different electronic load behavior that the state-of-the-art WECC-CLM cannot.

Comparison of the change in load demand between simulations 1 and 2-4 reveals that the electronic load model of the WECC-CLM is unresponsive to frequency variations. However, when the same load is modeled using the GSL load model, it reduces to less than 1/3rd of its initial value at its minimum point in the simulation.

Frequency profiles in simulations 2-4 suggest that it is possible to get grid support from loads for a short period of time and then restore loads without a significant impact on grid performance (in terms of frequency nadir and settling frequency). Duration of grid support is a unique feature of the proposed GSL model that is not found in the WECC-CLM.

Simulations 1-4 also show that voltage recovery is faster in simulations 2-4 when compared to simulation 1.

Compared to simulation 5, simulations 6-10 show higher frequency nadirs, lower overshoots, and shorter settling times indicating that even during faults, GSLs modeled using the proposed model can improve frequency response.

Finally, voltages at bus 5 in Figure 4 are almost identical between simulations 5-10. This is because by design the GSL model operates at a unity power factor and cannot provide reactive power support during faults.

D. Key Takeaways from Simulations

The results in Figure 3 and Figure 4 show that the developed GSL model works as expected under both generator trip and fault events, which are the two most commonly studied disturbances in power system analysis. The results also show that frequency response is significantly improved in the WECC 9-bus system when 25 MW out of the 315 MW total system load, i.e., 8% of the total load has grid-supportive properties. Improvement in voltages, however, was not observed with the GSL model. This is because of the unity power factor behavior simulated in the load model, which prevents it from providing reactive power support that is needed during faults. While a provision of reactive power support can be included in the GSL

model, it may not be reasonable to assume reactive power support from electronic loads because these are typically designed solely for unity power factor operation.

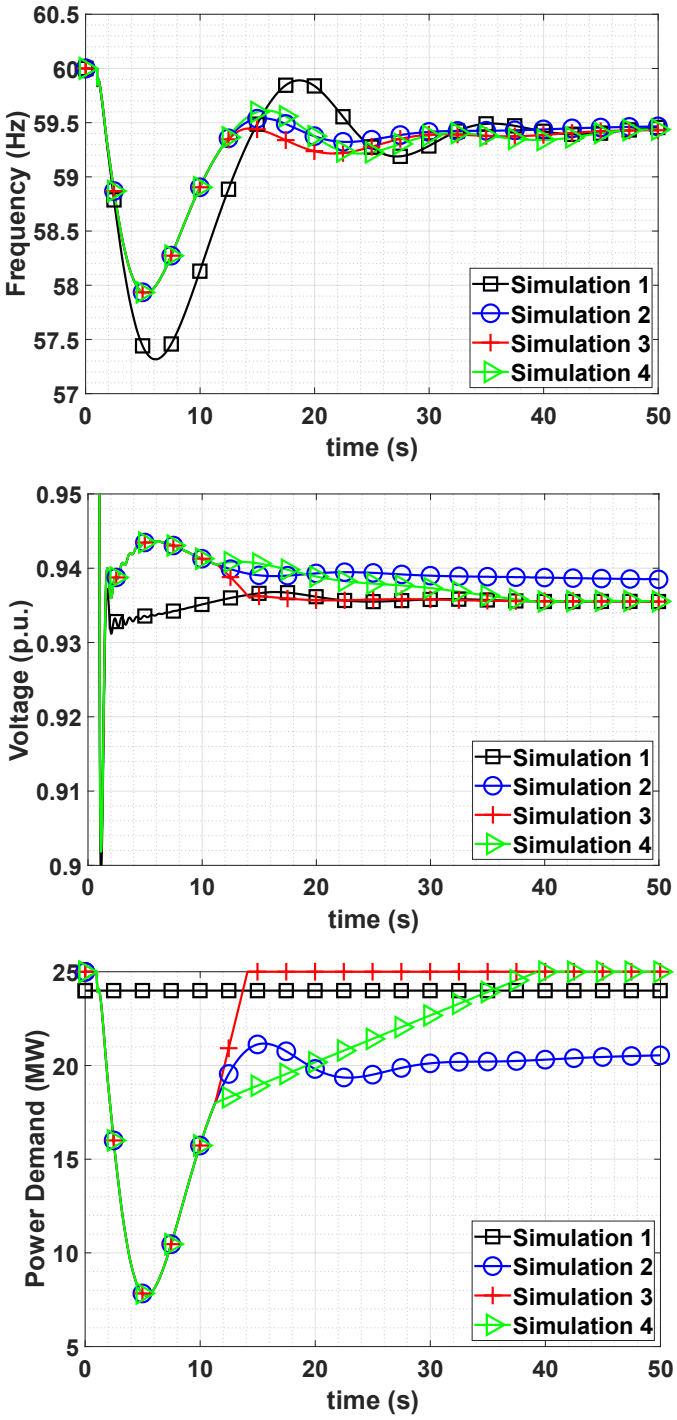

Figure 3. Results for Simulations 1-4. Frequencies at bus 5 (Top). Voltages at bus 5 (Middle). Power demand of load modeled w/o GSL behavior in simulation 1 and w/ GSL behavior in simulations 2-4 (Bottom).

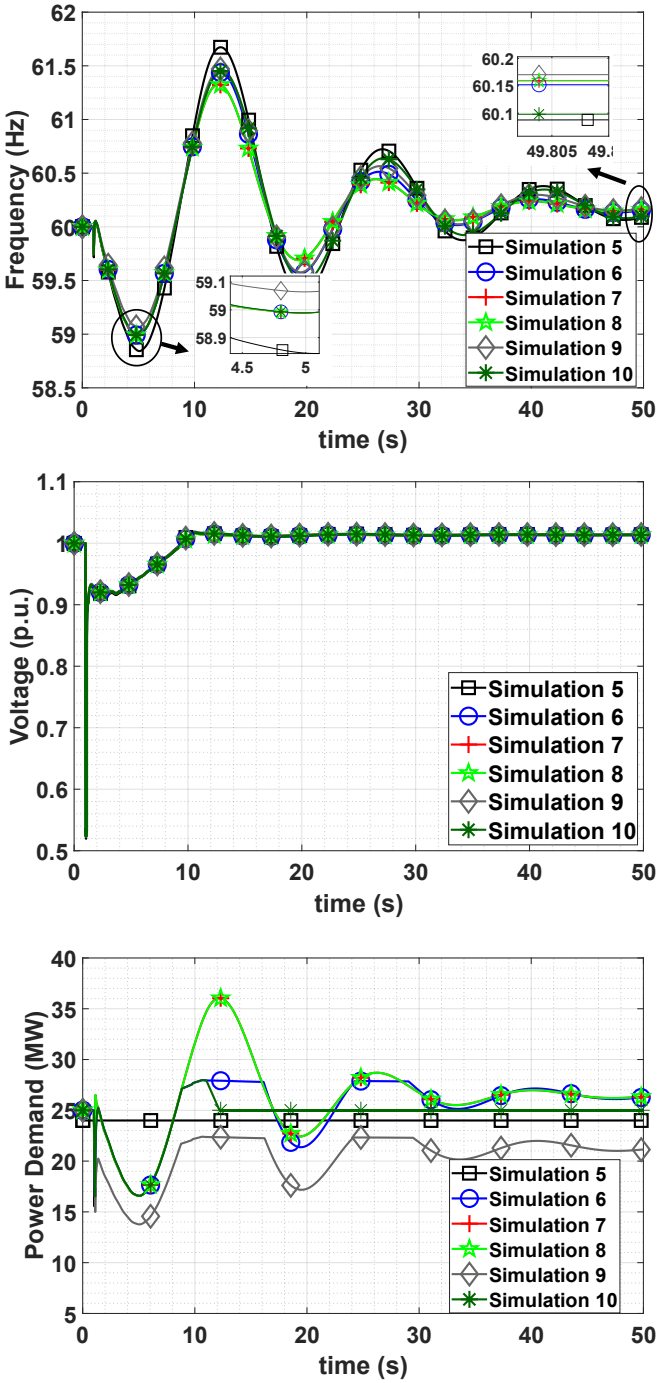

Figure 4. Results for Simulations 5-10. Frequencies at bus 5 (Top). Voltages at bus 5 (Middle). Power demand of load modeled w/o GSL behavior in simulation 5 and w/ GSL behavior in simulations 6-10 (Bottom).

VI. Application of the GSL Model on a 2000-bus Synthetic Power System Model

There were four objectives of performing this analysis:

1. Validate the performance of the GSL model on a realistic, utility-scale model. To this end, the 2000 bus synthetic model inspired by the ERCOT power system [42], hereafter referred to as the *ERCOT2K System*, was selected.
2. Validate the theoretical analysis of the GSL model performed in section IV.

3. Identify any potential adverse impacts on grid stability with hundreds of GSLs automatically responding to grid conditions.
4. Quantify the benefits of GSLs in enabling variable renewable integration.

A. Description of the ERCOT2K System

The ERCOT2K system is a modified version of the ACTIVSg2000 model, which is an entirely synthetic model built on the footprint of ERCOT [42]. The ACTIVSg2000 model is described in detail in [43].

Modifications were required because of some data errors in the GE-PSLF® dynamic file of the ACTIVSg2000 model. These errors were revealed when the dynamics data file was investigated after the no-disturbance dynamic simulations diverged. The primary reason for the divergence was the incorrect order of generator model parameters in the dynamics file that resulted in very high (some greater than 20%) stator resistance values. When these were fixed, the no-disturbance simulation did not diverge but significant transients in voltage and frequency profiles were observed. More changes in power flow and dynamics data were needed (e.g., correcting some generator and governor MVA bases because these were lower than the dispatched real powers) to ensure a "flat" no-disturbance run. The resulting modified ACTIVSg2000 model is called the ERCOT2K System in this paper. Several fault and generator trip events were simulated on the ERCOT2K system model, which resulted in numerically stable and logical results.

There were 98 generators (totaling to about 9.3 GW or 14% of the total load) whose dynamics were not modeled in the ACTIVSg2000 model. These were assumed to be variable renewable generators in the ERCOT2K System model and the "regc_a" and "reec_a" models of GE-PSLF®, with identical parameters for all generators, were used to simulate their dynamics [44].

B. Description of Simulations on the ERCOT2K System Model

Over 1100 GSLs were modeled using three droop coefficients - 4%, 2%, and 1% in the ERCOT2K System. Other parameters, except the MVA, were identical for all GSLs. MVA of each GSL was equal to its MVA in the power flow case. $Tpu_1, Tpu_2, Tpu_3, and\ Trst$ were 3, 2, 2 and 2 cycles, respectively. All other GSL parameters were the same as in Table III. Four GSL levels were modeled for each droop coefficient (5%, 10%, 15%, and 20% of the total load). Moreover, two sets of cases were created. One with renewable dynamic models added as discussed above, and the second with load reduced to around 53 GW (load was 67 GW earlier). To balance the decrease in load synchronous generators with the largest headroom were removed until only 2000 MW of aggregate headroom remained on the remaining synchronous generators (headroom was 27,000 MW earlier). This headroom was sufficient to compensate for the loss of the largest generator (generating around 1300 MW). The headroom on renewable generators was kept unchanged at 3000 MW. The renewable generation as a percentage of total load in the second set of cases increased to 18% (14% earlier). The total MVA of synchronous generators in the second set of cases decreased to 55,011 MVA (from 86,130 MVA in the first set of cases).

As shown in Table IV, a total of 30 simulations were run - 15 each for the two renewable generation levels. 13 simulations each were run with tripping of generator at bus 5262, which was dispatching 1212 MW (Case # 1-26). Two simulations each were run with solid three-phase-to-ground fault applied at bus 3048 (500 kV bus) at 15 seconds and cleared after 6 cycles (Case # 27-30).

Table IV. ERCOT2K System cases with GSLs

Case #	GSLs (MW)	GSL Droop	Frequency Response (MW/0.1 Hz)	Decrease in Frequency Deviation at Nadir (%)
1	0	4%	3360	-
2	3,356	4%	3430	8%
3	6,711	4%	3498	14%
4	10,066	4%	3756	20%
5	13,421	4%	3844	25%
6	3,356	2%	3526	16%
7	6,711	2%	3868	27%
8	10,066	2%	3994	35%
9	13,421	2%	4398	39%
10	3,356	1%	3875	27%
11	6,711	1%	4417	41%
12	10,066	1%	5041	47%
13	**13,421**	**1%**	**5352**	**50%**
14	0	4%	1938	-
15	2,641	4%	2054	8%
16	5,282	4%	2120	15%
17	7,922	4%	2224	21%
18	10,562	4%	2371	26%
19	2,641	2%	2119	15%
20	5,282	2%	2370	27%
21	7,922	2%	2572	37%
22	10,562	2%	2798	45%
23	2,641	1%	2369	28%
24	5,282	1%	2793	46%
25	7,922	1%	3163	55%
26	**10,562**	**1%**	**3552**	**59%**
27	0	4%	-	-
28	13,421	1%	-	-
29	0	4%	-	-
30	10,562	1%	-	-

C. ERCOT2K System Simulation Results

Plots comparing the settling frequencies and frequency nadirs obtained from simulation of cases 1-26 and those obtained after solving (28) are shown in Figure 5. Figure 6 shows the frequency plots for fault events (cases 27-30 of Table IV.

To find the exact roots of (28), the average values of parameters of the GSLs and the GGOV1 governors from the ERCOT2K System were substituted in its denominator. This resulted in one pair of complex conjugate roots with negative real parts and four real roots in the left half of the s-plane. Partial fractions expansion was used to obtain $\Delta\omega(t)$ from $\Delta\omega(s)$. Minimum values of $\Delta\omega(t)$ were used to obtain estimated frequency nadirs, whereas (30) was used to obtain estimates of settling frequencies.

Key observations from ERCOT2K System simulations are:

1. The estimated settling frequencies and frequency nadirs in cases 1-26 are close to the actual observed values from the detailed dynamic simulations (Mean absolute errors 0.004

Hz and 0.005 Hz, respectively). This validates the theoretical derivation and the expression for $\Delta\omega(s)$ in (28), which can be used to estimate the impact of hundreds of GSLs in a large-scale system under generator tripping events without running detailed dynamic simulations.

2. GSLs significantly improve the frequency response in the ERCOT2K System model. The improvement can be seen from Table IV, where at 14% renewable generation level frequency response increased from 3360 MW/0.1 Hz in the absence of GSLs to 5352 MW/0.1 Hz when 20% of the total load was modeled using the GSL model with 1% droop. Similarly, at 18% renewable generation level frequency response increased from 1938 MW/0.1 Hz in case 14 to 3552 MW in case 26, which is an increase of 83%.
3. The decreases in deviation from 60 Hz at frequency nadirs in the presence of GSLs is another indicator of improvement in frequency response. Table IV shows that frequency deviation at nadir decreased by 50% between cases 1 and 13, whereas it decreased by close to 60% between cases 14 and 26.
4. Figure 5 shows that GSLs significantly improve the frequency nadirs and settling frequencies at both 14% and 18% renewable generation levels. However, the more important observation is that for three GSL amounts and droop combinations (case 22 - 20% GSL, 2% droop; case 24 – 10% GSL, 1% droop; case 25 – 15% GSL, 1% drop, and case 26 – 20% GSL, 1% droop), the frequency nadir at 18% renewable levels is higher than the frequency nadir at 14% renewable generation level without GSLs (case 1). If the plot of settling frequencies is analyzed, case 26 (20% GSL, 1% droop) results in higher settling frequency than case 1.
5. Although GSLs improve settling frequencies at both 14% and 18% renewable generation levels, the absolute increase is less compared to frequency nadirs.
6. The impact of GSLs is also seen under fault events, although these operate at unity power factor. Figure 6 shows that in the presence of GSLs (cases 28 and 30), frequency nadirs are improved compared to the no GSL cases (cases 27 and 29) at both 14% and 18% renewable generation levels. Similar to the generator tripping cases, the increase in frequency nadir (0.05 Hz) is more (almost double) under 18% renewable generation level than the increase (0.02 Hz) at 14% renewable generation level.

The following conclusions about the GSLs can be drawn from these observations:

1. **GSLs support variable renewable integration in power systems.** GSLs significantly improve frequency response and their impact increases as variable renewable generation levels increase. The frequency nadir and settling frequency results show that a modest amount of GSL (10-20%) at 1-2% droop can help in achieving higher renewable generation levels at significantly lower synchronous generator headroom and inertia and without negatively impacting grid reliability. This is achieved without obtaining primary frequency response from renewable generators. The preserved headroom in renewable generators can be used to provide longer duration frequency support at secondary frequency response and regulation time frames. Moreover, the improvement in frequency response is observed for both generator tripping and fault events.
2. **Lower droop increases the effectiveness of GSLs.** If the percentage droop is reduced, fewer GSLs are needed to provide the same improvement in frequency nadirs.
3. **More improvement in frequency nadirs than in settling frequencies**. While GSLs improve both frequency nadir and settling frequencies, their impact is more prominent on frequency nadirs. This can be explained by the reduced deviation in frequency from the nominal value as new steady states are attained compared to the deviation in frequency near the frequency nadirs.

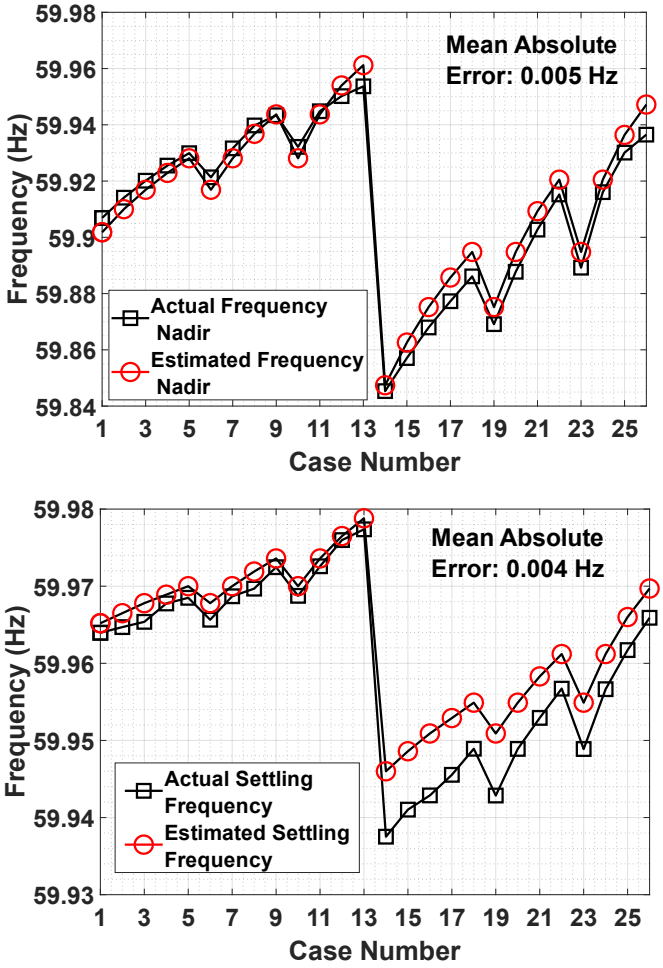

Figure 5. Estimated and actual frequencies for the generator trip cases in Table IV. Frequency nadirs (Top). Settling frequencies (Bottom).

VII. Conclusion and Next Steps

This paper proposed a novel idea of using electronic loads to provide grid support at transient timeframes and presented a new dynamic model for such grid-supportive loads. The gaps in the electronics load modelling capabilities of state-of-the-art load models were addressed in the developed GSL model and the model performance was validated under both generator tripping and fault events. The impact of the developed GSL model in improving the transient response and reliable integration of renewable energy was demonstrated on the WECC 9-bus system and the 2000 bus ERCOT2K System,

where over 1100 GSLs were modeled. Theoretical expressions to estimate the frequency response under generator tripping events in large power systems with hundreds of GSLs were also derived and their accuracy demonstrated by comparing the frequency nadirs and settling frequencies estimated from these expressions with those obtained from detailed dynamic simulations performed on the ERCOT 2K System.

The simulations performed on the ERCOT 2K system with over 1100 GSLs responding autonomously to locally measured voltage and frequencies show that if the grid-supportive capabilities are included in electronic loads as per the developed model, they can help in maintaining grid reliability at higher renewable penetration and at much lower synchronous generation availability. Moreover, renewable resources need to reserve lower headroom for providing grid support, which can improve their economics as they can inject more energy into the grid, or the headroom can be used for providing secondary frequency response and regulation reserve.

Future research will focus on implementing the developed GSL model in real equipment and in identifying the impact on the equipment's performance and end-users' utility. Further development of the GSL, such as exploring the potential for GSLs to provide voltage support during faults will also be pursued. It is hoped that this paper will further the research in making smart, inverter-based loads a key player in large-scale, reliable integration of variable renewable energy in power systems.

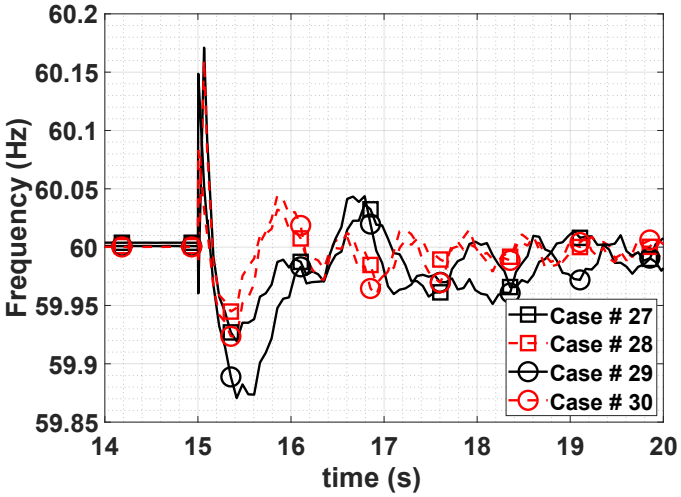

Figure 6. Average frequencies for fault events of Table IV.

APPENDIX I: QUALITATIVE DESCRIPTION OF THE GSL MODEL

The GSL model has five modules that work together to address the four limitations of the WECC-CLM. These are:

1. **Voltage and frequency measurements:** Voltage and frequency are measured using transducers with low pass filters to remove any numerical noise in the measurements.
2. **Frequency-power relationship:** The frequency-power relationship allows the reference power (P_{ref}) to be modulated by the changes in measured grid frequency (f_m). P_{ref} is kept fixed throughout the simulation at the pre-disturbance power being absorbed by the GSL. A parameter R, similar to the steady-state droop in generators, is used to translate deviation in frequency from the reference frequency (f_{ref}), into a change in the real power being absorbed by the load. R denotes the percentage change in frequency that will result in increase of 100% of the rated power of the load. If measured frequency falls below the user-defined reference frequency (60 Hz in this paper), more power than the initial power is absorbed by the load while a decrease in grid frequency results in less than the initial power being absorbed.
3. **Inverter delays and current limits:** This block was inspired by the similar block in the $regc\_a$ model, which is designed to represent the interface of inverter-based generators with the power system in the WECC 2nd generation renewable models [44]. It is meant to represent the entirety of delays (T_g) in the inverter when translating the commanded power from the frequency block into the current that should be absorbed from the network. It also applies the maximum (I_{max}) and minimum (I_{min}) current limits to the commanded current. Provision for negative I_{min} is provided to enable the possibility of a GSL with energy storage element in it (e.g., a capacitor or a battery) that can inject power in the grid. Another parameter, $rrpwr$, is also associated with this block that limits the rate of recovery of load to a user-defined value after the commanded power becomes zero.
4. **Load restoration:** The purpose of this block is to enable load restoration sometime after the disturbance. This allows an electronic load to provide grid support for a specified duration after the disturbance and then restore its initial demand at the user-defined rate. GSL behavior is disabled when (i) the deviation in load from the initial value exceeds 5% (user-defined) and (ii) after the grid support duration ($Tlrest$) is exceeded. Then, the load is linearly ramped to its initial value at the user-defined rate ($rrate$).
5. **Voltage dependent load tripping logic:** This block is designed to trip a fraction of the electronic load if the voltage is low and within one of the specified ranges. Both definite time (i.e., fixed load trip time irrespective of the low voltage range) and inverse time (i.e., decreasing load trip time with decreasing low voltage ranges) characteristics can be simulated. The relay trips a fraction of load after the voltage stays in a low voltage band for more than a specified time This time is reset, and load fraction is not changed if the voltage recovers above the maximum voltage of the range for more than a specified reset time. Figure 1 shows this logic.

APPENDIX II: LONG EXPRESSIONS USED IN THE THEORETICAL ANALYSIS

Symbol	Expression
$expr1$	$\left(\frac{1}{s}\right)\left(1+\frac{R_{G_{eq}}}{1+sT_{pelec}}.K_{turb}\left(K_{pgov}+\frac{K_{igov}}{s}\right)\left(\frac{1}{1+sT_{act}}\right)\left(\frac{1}{1+sT_b}\right)\right)$
$expr2$	$\left(s2H_{eq}+\left(K_{turb}\left(1+\frac{R_{G_{eq}}}{1+sT_{pelec}}.\frac{R_{GSL_{eq}}}{1+sT_G}\right)\left(K_{pgov}+\frac{K_{igov}}{s}\right)\left(\frac{1}{1+sT_{act}}\right)\left(\frac{1}{1+sT_b}\right)+\frac{R_{GSL_{eq}}}{1+sT_G}\right)\right)$
a_5	1
a_4	$\frac{1}{T_{pelec}}+\frac{1}{T_a}+\frac{1}{T_g}+\frac{1}{T_b}$
a_3	$\frac{1}{T_{pelec}T_g}+\frac{1}{T_aT_g}+\frac{1}{T_aT_b}+\frac{1}{T_bT_{pelec}}+\frac{1}{T_aT_{pelec}}+\frac{1}{T_bT_g}$
a_2	$\frac{1}{T_aT_{pelec}T_g}+\frac{1}{T_aT_bT_g}+\frac{1}{T_aT_bT_{pelec}}+\frac{1}{T_bT_gT_{pelec}}+\frac{Kp*Kt*r}{T_aT_bT_{pelec}}$
a_1	$\frac{Kp*Kt*r}{T_aT_bT_{pelec}T_g}+\frac{Ki*Kt*r}{T_aT_bT_{pelec}}+\frac{1}{T_aT_bT_{pelec}T_g}$
a_0	$\frac{Ki*Kt*r}{T_aT_bT_{pelec}T_g}$
b_6	1
b_5	$\left(\frac{1}{T_p}+\frac{1}{T_g}+\frac{1}{T_b}+\frac{1}{T_a}+\frac{Kt}{2H_{eq}}\right)$
b_4	$\left(\frac{1}{T_{pelec}T_g}+\frac{1}{T_aT_g}+\frac{1}{T_aT_b}+\frac{1}{T_bT_{pelec}}+\frac{1}{T_aT_{pelec}}+\frac{1}{T_bT_g}+\frac{R_{GSL_{eq}}}{2H_{eq}T_g}\right)$
b_3	$\left(\frac{1}{T_aT_{pelec}T_g}+\frac{1}{T_aT_bT_g}+\frac{1}{T_aT_bT_{pelec}}+\frac{1}{T_bT_gT_{pelec}}+\frac{KpKt}{2H_{eq}T_aT_b}+\frac{R_{GSL_{eq}}}{2H_{eq}}\left(\frac{1}{T_{pelec}T_g}+\frac{1}{T_bT_g}+\frac{1}{T_aT_g}\right)\right)$
b_2	$\left(\frac{1}{T_aT_bT_gT_{pelec}}+\left(\frac{R_{GSL_{eq}}}{2H_{eq}}\right)\left(\frac{1}{T_aT_{pelec}T_g}+\frac{1}{T_aT_bT_g}+\frac{1}{T_bT_gT_{pelec}}\right)+\frac{K_pK_t}{2H_{eq}}\left(\frac{1}{T_aT_bT_{pelec}}+\frac{1}{T_aT_bT_g}\right)+\frac{K_iK_t}{2H_{eq}T_aT_b}\right)$
b_1	$\left(\frac{R_{GSL_{eq}}}{2H_{eq}T_aT_bT_gT_{pelec}}+\frac{K_pK_t}{2H_{eq}T_aT_bT_gT_{pelec}}+\frac{K_iK_t}{2H_{eq}}\left(\frac{1}{T_aT_bT_{pelec}}+\frac{1}{T_aT_bT_g}\right)+\frac{K_pK_trR_{GSL_{eq}}}{2H_{eq}T_aT_bT_gT_{pelec}}\right)$
b_0	$\frac{K_iK_t+K_iK_trR_{GSL_{eq}}}{2H_{eq}T_aT_bT_gT_{pelec}}$

VIII. REFERENCES

[1] Federal Electricity Regulatory Commission (FERC), *Essential Reliability Services and the Evolving Bulk-Power System—Primary Frequency Response*. 2018. [Online]. Available: https://www.ferc.gov/whats-new/comm-meet/2018/021518/E-2.pdf

[2] "IEEE Standard for Interconnection and Interoperability of Distributed Energy Resources with Associated Electric Power Systems Interfaces–Amendment 1: To Provide More Flexibility for Adoption of Abnormal Operating Performance Category III," *IEEE Std 1547a-2020 Amend. IEEE Std 1547-2018*, pp. 1–16, Apr. 2020, doi: 10.1109/IEEESTD.2020.9069495.

[3] "California Utilities Define New Smart Inverter Capabilities - IEEE Smart Grid." https://smartgrid.ieee.org/newsletters/june-2019/california-utilities-define-new-smart-inverter-capabilities (accessed Jul. 19, 2021).

[4] WECC Renewable Energy Modeling Task Force, "WECC Solar Plant Dynamic Modeling Guidelines," Western Electricity Coordinating Council, Apr. 2014. [Online]. Available: https://www.wecc.org/reliability/wecc%20solar%20plant%20dynamic%20modeling%20guidelines.pdf

[5] WECC Renewable Energy Modeling Task Force, "WECC Wind Power Plant Dynamic Modeling Guide," Western Electricity Coordinating Council, Apr. 2014. [Online]. Available: https://www.wecc.biz/Reliability/WECC%20Wind%20Plant%20Dynamic%20Modeling%20Guidelines.pdf

[6] Electric Power research Institute, *OpenDSS*. Electric Power research Institute. [Online]. Available: https://www.epri.com/pages/sa/opendss

[7] "The Shift towards Energy Efficient Appliances Continues to Drive Growth in the Home Appliance Market," *Assembly*, Aug. 01, 2017. [Online]. Available: https://www.assemblymag.com/articles/94872-the-shift-towards-energy-efficient-appliances-continues-to-drive-growth-in-the-home-appliance-market

[8] U.S. Department of Energy, "Quadrennial Technology Review: An Assessment of Energy Technologies and Research Opportunities," Sep. 2015. [Online]. Available: https://www.energy.gov/quadrennial-technology-review-2015

[9] F. Shariatzadeh, P. Mandal, and A. K. Srivastava, "Demand response for sustainable energy systems: A review, application and implementation strategy," *Renew. Sustain. Energy Rev.*, vol. 45, pp. 343–350, May 2015, doi: 10.1016/j.rser.2015.01.062.

[10] I. Hussain, S. Mohsin, A. Basit, Z. A. Khan, U. Qasim, and N. Javaid, "A Review on Demand Response: Pricing, Optimization, and Appliance Scheduling," *Procedia Comput. Sci.*, vol. 52, pp. 843–850, Jan. 2015, doi: 10.1016/j.procs.2015.05.141.

[11] M. S. Hossan *et al.*, "Deployment of Conservation Voltage Reduction in Sample Feeders: A Systemwide Energy-Savings Analysis," *IEEE Ind. Appl. Mag.*, vol. 27, no. 2, pp. 36–46, Mar. 2021, doi: 10.1109/MIAS.2020.3024487.

[12] Z. Wang and J. Wang, "Review on Implementation and Assessment of Conservation Voltage Reduction," *IEEE Trans. Power Syst.*, vol. 29, no. 3, pp. 1306–1315, May 2014, doi: 10.1109/TPWRS.2013.2288518.

[13] P. K. Sen and K. H. Lee, "Conservation Voltage Reduction Technique: An Application Guideline for Smarter Grid," *IEEE Trans. Ind. Appl.*, vol. 52, no. 3, pp. 2122–2128, May 2016, doi: 10.1109/TIA.2016.2525937.

[14] L. G. Swan and V. I. Ugursal, "Modeling of end-use energy consumption in the residential sector: A review of modeling techniques," *Renew. Sustain. Energy Rev.*, vol. 13, no. 8, pp. 1819–1835, Oct. 2009, doi: 10.1016/j.rser.2008.09.033.

[15] M. G. Prina, G. Manzolini, D. Moser, B. Nastasi, and W. Sparber, "Classification and challenges of bottom-up energy system models - A review," *Renew. Sustain. Energy Rev.*, vol. 129, p. 109917, Sep. 2020, doi: 10.1016/j.rser.2020.109917.

[16] S. de la Rue du Can *et al.*, "Modeling India's energy future using a bottom-up approach," *Appl. Energy*, vol. 238, pp. 1108–1125, Mar. 2019, doi: 10.1016/j.apenergy.2019.01.065.

[17] R. Kadian, R. P. Dahiya, and H. P. Garg, "Energy-related emissions and mitigation opportunities from the household sector in Delhi," *Energy Policy*, vol. 35, no. 12, pp. 6195–6211, Dec. 2007, doi: 10.1016/j.enpol.2007.07.014.

[18] C. Cresswell and S. Djokic, "Representation of directly connected and drive-controlled induction motors. Part 2: Three-phase load models," in *2008 18th International Conference on Electrical Machines*, Sep. 2008, pp. 1–6. doi: 10.1109/ICELMACH.2008.4800119.

[19] A. Bokhari *et al.*, "Experimental Determination of the ZIP Coefficients for Modern Residential, Commercial, and Industrial Loads," *IEEE Trans. Power Deliv.*, vol. 29, no. 3, pp. 1372–1381, Jun. 2014, doi: 10.1109/TPWRD.2013.2285096.

[20] Y. Baghzouz and C. Quist, "Composite load model derivation from recorded field data," in *IEEE Power Engineering Society. 1999 Winter Meeting (Cat. No.99CH36233)*, Jan. 1999, vol. 1, pp. 713–718 vol.1. doi: 10.1109/PESW.1999.747544.

[21] Z. Guo, Z. J. Wang, and A. Kashani, "Home Appliance Load Modeling From Aggregated Smart Meter Data," *IEEE Trans. Power Syst.*, vol. 30, no. 1, pp. 254–262, Jan. 2015, doi: 10.1109/TPWRS.2014.2327041.

[22] L. M. Hajagos and B. Danai, "Laboratory measurements and models of modern loads and their effect on voltage stability studies," *IEEE Trans.*

Power Syst., vol. 13, no. 2, pp. 584–592, May 1998, doi: 10.1109/59.667386.

[23] Y. Liu and V. Vittal, "Distribution side mitigation strategy for fault induced delayed voltage recovery," in *2014 IEEE PES General Meeting | Conference Exposition*, Jul. 2014, pp. 1–5. doi: 10.1109/PESGM.2014.6939041.

[24] Y. Liu *et al.*, "Detailed Modeling of Residential End-Use Motor Load and Protection for Distribution System Transient Study," in *2019 IEEE Power Energy Society Innovative Smart Grid Technologies Conference (ISGT)*, Feb. 2019, pp. 1–5. doi: 10.1109/ISGT.2019.8791650.

[25] M. Rylander, W. M. Grady, A. Arapostathis, and E. Powers, "A voltage sag-based procedure for determining transient stability models of conventional loads," in *IEEE Electric Ship Technologies Symposium, 2005.*, Jul. 2005, pp. 321–324. doi: 10.1109/ESTS.2005.1524695.

[26] Q. Huang *et al.*, "A generic modeling and development approach for WECC composite load model," *Electr. Power Syst. Res.*, vol. 172, pp. 1–10, Jul. 2019, doi: 10.1016/j.epsr.2019.02.027.

[27] "Reliability Guideline Parameterization of the DER_A Model," North American Electric Reliability Corporation, Sep. 2019. Accessed: Feb. 14, 2021. [Online]. Available: https://www.nerc.com/comm/PC_Reliability_Guidelines_DL/Reliability_Guideline_DER_A_Parameterization.pdf

[28] R. W. Kenyon, B. Mather, and B.-M. Hodge, "Coupled transmission and distribution simulations to assess distributed generation response to power system faults," *Electr. Power Syst. Res.*, vol. 189, p. 106746, Dec. 2020, doi: 10.1016/j.epsr.2020.106746.

[29] Q. Huang and V. Vittal, "Integrated Transmission and Distribution System Power Flow and Dynamic Simulation Using Mixed Three-Sequence/Three-Phase Modeling," *IEEE Trans. Power Syst.*, vol. 32, no. 5, pp. 3704–3714, Sep. 2017, doi: 10.1109/TPWRS.2016.2638910.

[30] Irina Green, "CMPLDWG Composite Model with Distributed Generation DER_A CAISO Assessment," presented at the NERC Load Modeling Task Force Meeting, May 2018. [Online]. Available: https://www.nerc.com/comm/PC/LoadModelingTaskForceDL/CMPLDWG_DER_A_CAISO_NERC.pdf

[31] North American Electrical Reliability Corporation, "Technical Reference Document - Dynamic Load Modeling." Dec. 2016. [Online]. Available: https://www.nerc.com/comm/PC/LoadModelingTaskForceDL/Dynamic%20Load%20Modeling%20Tech%20Ref%202016-11-14%20-%20FINAL.PDF

[32] Y. Xu, W. Lu, kun wang, C. Li, and W. Aslam, "Sensitivity of Low-Voltage Variable-Frequency Devices to Voltage Sags," *IEEE Access*, vol. 7, pp. 2068–2079, 2019, doi: 10.1109/ACCESS.2018.2885402.

[33] S. M. H. Rizvi, K. S. Sajan, and A. K. Srivastava, "Real-Time Parameter Tracking of Power-Electronics Interfaced Composite ZIP Load Model," *IEEE Trans. Smart Grid*, pp. 1–1, 2021, doi: 10.1109/TSG.2021.3119507.

[34] Y. Lin, Y. Wang, J. Wang, and D. Shi, "Tensor-Based Parameter Reduction of Dynamic Load Models with Variable Frequency Drive," *IEEE Trans. Power Syst.*, pp. 1–1, 2021, doi: 10.1109/TPWRS.2021.3100563.

[35] Z. Ma, B. Cui, Z. Wang, and D. Zhao, "Parameter Reduction of Composite Load Model Using Active Subspace Method," *IEEE Trans. Power Syst.*, vol. 36, no. 6, pp. 5441–5452, Nov. 2021, doi: 10.1109/TPWRS.2021.3078671.

[36] J. Xie *et al.*, "Imitation and Transfer Q-Learning-Based Parameter Identification for Composite Load Modeling," *IEEE Trans. Smart Grid*, vol. 12, no. 2, pp. 1674–1684, Mar. 2021, doi: 10.1109/TSG.2020.3025509.

[37] F. Bu, Z. Ma, Y. Yuan, and Z. Wang, "WECC Composite Load Model Parameter Identification Using Evolutionary Deep Reinforcement Learning," *IEEE Trans. Smart Grid*, vol. 11, no. 6, pp. 5407–5417, Nov. 2020, doi: 10.1109/TSG.2020.3008730.

[38] X. Wang, Y. Wang, D. Shi, J. Wang, and Z. Wang, "Two-Stage WECC Composite Load Modeling: A Double Deep Q-Learning Networks Approach," *IEEE Trans. Smart Grid*, vol. 11, no. 5, pp. 4331–4344, Sep. 2020, doi: 10.1109/TSG.2020.2988171.

[39] P. Mitra, D. Ramasubramanian, A. Gaikwad, and J. Johns, "Modeling the Aggregated Response of Variable Frequency Drives (VFDs) for Power System Dynamic Studies," *IEEE Trans. Power Syst.*, vol. 35, no. 4, pp. 2631–2641, Jul. 2020, doi: 10.1109/TPWRS.2020.2966820.

[40] L. Pereira, J. Undrill, D. Kosterev, D. Davies, and S. Patterson, "A new thermal governor modeling approach in the WECC," *IEEE Trans. Power Syst.*, vol. 18, no. 2, pp. 819–829, May 2003, doi: 10.1109/TPWRS.2003.811007.

[41] "WSCC 9-Bus System - Illinois Center for a Smarter Electric Grid (ICSEG)." https://icseg.iti.illinois.edu/wscc-9-bus-system/ (accessed Jan. 28, 2022).

[42] "Electric Grid Test Case Repository." https://electricgrids.engr.tamu.edu/ (accessed Feb. 15, 2021).

[43] T. Xu, A. B. Birchfield, and T. J. Overbye, "Modeling, Tuning, and Validating System Dynamics in Synthetic Electric Grids," *IEEE Trans. Power Syst.*, vol. 33, no. 6, pp. 6501–6509, Nov. 2018, doi: 10.1109/TPWRS.2018.2823702.

[44] WECC Renewable Energy Modeling Task Force, "WECC Solar Plant Dynamic Modeling Guidelines," Western Electricity Coordinating Council, Apr. 2014. [Online]. Available: https://www.wecc.org/reliability/wecc%20solar%20plant%20dynamic%20modeling%20guidelines.pdf

IX. Biographies

Himanshu Jain (S'15-16, M'17) is an Assistant Professor in the Department of Hydro and Renewable Energy at the Indian Institute of Technology, Roorkee. He has over 10 years of combined research and industry experience in modelling and analyzing the impacts of integrating high levels of renewable energy in power systems. Before joining IIT Roorkee, Dr. Jain worked as a Senior Research Engineer and Research Engineer at the National Renewable Energy Laboratory (NREL), Golden, Colorado, USA from February 2017 to February 2021. His research is focused on focused on improving the reliability and resilience of power systems under high penetration levels of renewable energy resources at multiple temporal and spatial scales. Dr. Jain holds PhD, MS, and B. Tech degrees in Electrical Engineering from Virginia Tech, the University of Texas at Arlington, and G.B. Pant University of Agriculture & Technology, respectively.

Barry Mather (S'03–M'10–SM'14) received the B.S. and M.S. degrees in electrical engineering from the University of Wyoming, Laramie, WY, USA, in 2001 and 2004, respectively, and the Ph.D. degree in electrical engineering from the University of Colorado, Boulder, CO, USA, in 2010. Since 2010, he has been with the Power Systems Engineering Center, National Renewable Energy Laboratory, Golden, CO, USA, where he currently leads multiple research projects focused on the modeling and mitigation of photovoltaic integration impacts on interconnected distribution power systems. He also leads a research group focused on the interconnection of renewable generation and other grid technologies to the power system including a broad spectrum of research focus areas from power electronics development to informing and developing DER interconnection standards.

Akshay Kumar Jain (Student Member, IEEE) received the M.S. degree in electrical engineering (EE) from Virginia Tech where he is currently working towards the Ph.D. degree in EE. He previously worked as a research engineer at NREL. He was the recipient of RD100 and Federal Laboratory Consortium's Notable Technology Development awards in 2019. His research interests include modeling, stability analysis and optimal control of electric grids with high penetration of power electronics interfaced resources.

Samuel F. Baldwin (M'84) received the B.A. degrees in physics and in mathematics from University of Oregon and the M.S. and Ph.D. degrees in physics from the University of Maryland, College Park, USA. He is currently the Chief Science Officer for the Office of Energy Efficiency and Renewable Energy at the U.S. Department of Energy. His research interests cover a wide range of energy efficiency and renewable energy technologies and their systems integration.